Control of a double impacting mechanical oscillator using displacement feedback

E. Gutiérrez* D. K. Arrowsmith†

June 4, 2003

Keywords: impacting systems, resonance, control, anti-control, feedback, chaotic regime.

Abstract

A model which allows a double impacting regime for a particle undergoing simple harmonic motion is considered in some detail. The behaviour of the particle in the weak spring limit is considered. Symmetries of the motion are found and the extent of the resonant dynamical behaviour is considered. Control equations are developed and strategies are described for both the preservation and the annihilation of resonant periodic orbits.

1 Motivation and Background

The model we consider in this paper is a representation of a doubly constrained impacting system. It is motivated by a generic problem in engineering associated with the servo-assisted control of mechanical systems with slack. The original motivation for this study was to understand the nature of non-linear resonances associated with the interaction of servo-hydraulic pistons with multi-storey buildings during full-scale laboratory simulations used to analyse their seismic behaviour [8, 15, 16]. During tests, the structural interaction of the building with the pistons can cause spurious resonant vibrations which, ideally, should not be present during the experiments. In this paper we conjecture that the underlying causes that generate such behaviour are the mechanical discontinuities that are latent in all mechanisms, and that such phenomena is usually activated when the system is being driven in such a manner that either high positioning accuracy or performance is required. Thus this paper targets the general –engineering– background where these mechanical systems are common, and is intended to be applied to the wider problem of response and control of servo-actuated mechanisms: in other words, our investigations may be applicable to problems where physical objects must be manipulated by feedback assisted actuators. Although practical engineering solutions can be found for such non-linear resonances, the underlying nature of their cause and the range of dimensional scales at which they manifest themselves is so broad that it warrants a formal description in mathematical terms.

We analyze the control of a mathematical model of the laboratory set-up of a double-impacting system. Such basic doubly constrained systems are applicable to a wide variety of mechanisms and so have been widely studied in various forms in the literature [1, 12, 23] where the generic behaviour in terms of the existence of periodic and quasi-periodic orbits and their stability and bifurcations has been extensively examined. In particular, formal study of the intuitive concepts of impacts that just miss or arrive at their physical constraint at near zero normal velocity has been important. The behaviour of such orbits may be critically defined by a bifurcation variously referred to as

*European Commission Joint Research Centre, Ispra, Italy.
†Mathematics Research Centre, School of Mathematical Sciences, Queen Mary, University of London, London E1 4NS, UK.

a *grazing* [4, 11, 17] or a *border* bifurcation [18]. It has been shown that grazing bifurcations are one of the main routes to complex chaotic and intermittent behaviour the cause of which has been studied in generic –usually single sided impact systems– [4, 7, 13]. In our study we shall discuss the effect of how grazing impacts limit the stability regions of certain periodic orbits.

In the studies mentioned above the mechanical systems are passive in the sense that no attempt is made to control the orbit once the parametric configuration has been set. The control of chaotic non-linear systems has been widely discussed in the literature on the basis of the, so-called OGY method [19], and work has already been published on the control of impact systems [10, 20, 25]. However, in practical engineering applications the positioning systems of a servo-actuated mechanism require a displacement feedback term which is a key part of the study in this paper.

1.1 Condensation of the full-scale model

Empirical observations from a number of experiments on complex full-scale structures tested at the JRC's laboratory, suggested that the essential dynamical instability that created undesired resonances were probably being generated by a single disturbed piston whose unstable behaviour about some steady, quasi-static, movement generated stable impact resonances that propagated through the structure and were later picked up and amplified by the remaining pistons. Given that such a complex system was amenable neither to repeated experimental parametric analysis nor mathematical tractability, a bench model was constructed. The transformation of how a test piston discontinuously connected to a reinforced concrete structure reverts to a tractable impact oscillator for experimentation is seen in Fig. 1(a). The bench model consists of two rigidly connected steel plates mounted to the end of a servo-actuated piston. A steel mass with two rubber impact tips is mounted on a steel leaf spring that fits loosely between the steel plates. The ends of the leaf spring are rigidly connected to the test machine frame. The gap in the connecting plates may be very small compared to the overall size of the specimen; but the effective size of the gap is unimportant, for as we shall show, it is the gap size normalised by the amplitude of the overall range of piston motion that is of interest. We note that although the gap is nominally located at the piston connecting devices, in fact it serves to represent the discontinuity of the piston with some massive object with which it can interact. Thus, even if the piston were tightly connected to a part of the structure, the latter may have developed some crack in such a manner that two substructures are generated –one rigidly connected to the piston and the other separated from both of them by a small gap. Qualitatively the effect is the same.

2 The mechanical model

The simplest mathematical model which encompasses the laboratory behaviour is that of a constrained double impact oscillator (see Fig. 1(b)). The model consists of a particle attached to fixed points by two light springs. The particle can oscillate, without friction, within a gap defined by two rigid walls a fixed distance apart. This set-up is used to represent a slack connection between a piston and the object it is supposed to move in some cyclic fashion; in this sense the spring represents the columns of a swaying building whereas the mass represents the mass of the floor where it is connected to the piston clamping devices, here represented by two adjacent walls.

We can scale the gap size G between the rigid walls to be 2. Each wall oscillates according to a sinusoidal reference motion with frequency Ω of the form $W_r = A\sin\Omega t$. Dissipation can be introduced during impacting via a restitution coefficient r where $0 < r \leq 1$. Finally, the motions of the wall and the particle are coupled via a displacement feedback term, βx, where x is the displacement of the particle from its equilibrium. Thus the actual wall motions are given by

$$W^{\pm}(t) = \pm 1 + A\sin\Omega t + \beta x(t). \tag{1}$$

There are two essential components to the motion of the particle. The *freeflight* motion between the rigid walls is simple harmonic with frequency ω and determined by $\ddot{x} = -\omega^2 x$. Thus

$$x_1 = x_0\cos(\omega t) + y_0\sin(\omega t)/\omega, y_1 = -x_0\omega\sin(\omega t) + y_0\cos(\omega t) \tag{2}$$

for the initial and final conditions of (x_0, y_0, t_0) and (x_1, y_1, t_1) where $y = \dot{x}$. The ratio ω/Ω is the critical parameter and it can be seen that, with a suitable rescaling of time, $\Omega = 1$ can be assumed. At impact with either W^+ or W^-, it is assumed that the wall is massive and has an unchanged velocity. The velocities of the particle, y_0^+ and y_0^- immediately before and after the impact at $t = t_0$, are related by the coefficient of restitution equation

$$y_0^+ = -(r(1-\beta) - \beta)y_0^- + (1+r)\dot{W}_r(t_0). \tag{3}$$

Note that the introduction of a feedback term βx effects a change from the *actual* coefficient of restitution r to an *effective* coefficient of restitution

$$\hat{r} = r(1-\beta) - \beta. \tag{4}$$

Furthermore, it should be noted that the choice of a negative β could render $\hat{r} > 1$.

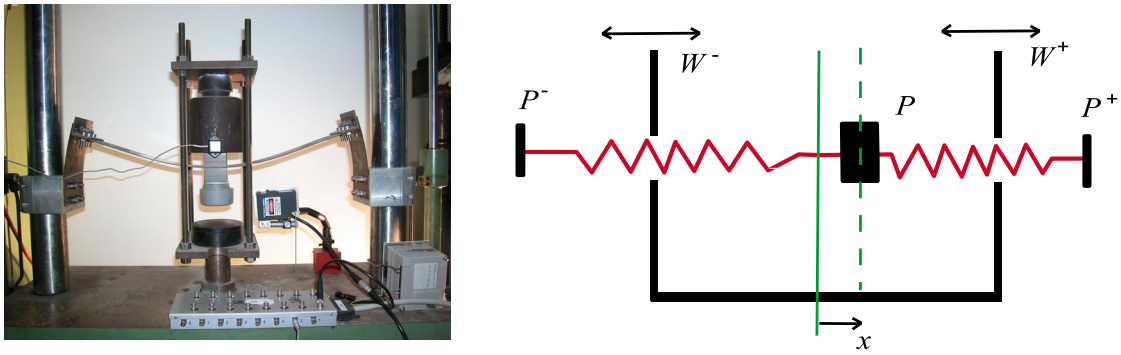

(a) (b)

Figure 1: (a) The double impacting bench model; (b) The walls W^+ and W^- oscillate simple harmonically with frequency Ω. The particle P is attached to the light springs fixed at points P^+, P^- and oscillates simple harmonically between the walls W^+ and W^-.

The double impacting regime we consider is an alternating one where

$$W^{\pm}(t_j) = x(t_j) \qquad \text{and} \qquad W^{\mp}(t_{j+1}) = x(t_{j+1}), \tag{5}$$

for $j = 0, 1, 2, 3, \ldots$ if subsequent impacts occur at $t = t_0, t_1, t_2, \ldots$. The detail of the free-flight and impact equations and the deduction of the linearised control systems is given in Appendix 1.

2.1 The Poincaré map

The orbits of interest in this paper are those which sequentially impact on alternate walls. The behaviour of such orbits can be investigated using a Poincaré map which takes dynamical information of the state of the system at discrete times. The simplest approach is to take stroboscopic information at the rate Ω, the frequency of the walls. In Fig. 2, we show a sample of orbits and their position in a stroboscopic Poincaré section taken for a standard conservative case $(r, \beta) = (1, 0)$, with amplitude $A = 0.1$ and frequency ratio $\omega/\Omega = 1/2\pi$. We plot the coordinates (x_t, y_t) for $t = 0, 1, 2, \ldots$ We notice various regions of periodicity such as (i) (1,1)-impact orbits as well and (ii) pure non-impact harmonic orbit it surrounded by areas of ergodic orbits. These, in turn, are surrounded by bands of quasi-periodic motions associated to periodic orbits having more than one bounce per wall period. Higher order n-impact orbits exist at higher impact velocities. In general the topological features of the phase diagram will depend on the amplitude and frequency ratios that prevail. We notice that the map is symmetric about the velocity axis for $r = \hat{r} = 1$, however, symmetry is destroyed when dissipation ($r < 1$) is introduced. An alternative approach to the stroboscopic map is to consider a Poincaré map which records the subsequent times of impact and the incident velocities on a chosen wall, [4, 24, 25]. This information, together with a knowledge of the feedback coefficient β, which defines the wall position at impact, then gives instantaneous velocity and position thus enabling the subsequent dynamics to be determined. We use the latter approach in this paper.

3 Resonant orbits

3.1 Space- and time- symmetric periodic orbits

We are interested in the case where the period of oscillation of the particle between successive impacts on the same wall is a multiple of the period $2\pi/\Omega$ of the oscillation of the wall. *Fundamental* period-1 orbits occur when there

are consecutive bounces on alternate walls at times $t_j = t_0 + j\pi/\Omega$. The most obvious examples of such orbits are found by imposing both space- and time- symmetries.

They are then either

- "trough-trough" (T) period-1 orbits that can be generated by two segments:

$$x(t) = \begin{cases} \frac{(1+A)\sin\omega t}{\sin\omega\pi/(2\Omega)}, & t \in [-\pi/(2\Omega), \pi/(2\Omega)], \\ -\frac{(1+A)\sin\omega(t-2\pi/(2\Omega))}{\sin\omega\pi/(2\Omega)}, & t \in [\pi/(2\Omega), 3\pi/(2\Omega)]. \end{cases} \tag{6}$$

  All other trajectories are obtained from translating either of these segments in time by $2\pi/\Omega$.

- the corresponding segments which generate the "peak-peak" (P) orbits are described by

$$x(t) = \begin{cases} \frac{(1-A)\sin\omega(t-\pi/\Omega)}{\sin\omega\pi/(2\Omega)}, & t \in [\pi/(2\Omega), 3\pi/(2\Omega)], \\ -\frac{(1-A)\sin\omega(t-2\pi/\Omega)}{\sin\omega\pi/(2\Omega)}, & t \in [3\pi/(2\Omega), 5\pi/(2\Omega)]. \end{cases} \tag{7}$$

Note that the P orbits can be obtained from the T orbits by simply allowing a negative amplitude for A. Also, there exist corresponding fundamental period-n P and T orbits for $n > 1$. For odd n, the "trough-trough" orbit is generated by

$$x(t) = (1+A)\sin\omega(t - (n-1)\pi/(2\Omega))/\sin n\pi\omega/(2\Omega), \tag{8}$$

$t \in [-\pi/(2\Omega), (2n-1)\pi/(2\Omega)]$, and the "peak-peak" orbit is given by

$$x(t) = (1-A)\sin\omega(t - (n+1)\pi/(2\Omega))/\sin n\pi\omega/(2\Omega), \tag{9}$$

$t \in [\pi/(2\Omega), (2n+1)\pi/(2\Omega)]$. Reflections in the x-axis of (8) and (9) and time translation by appropriate multiples of $n\pi/\Omega$ give the other segments. The orbit has consecutive wall impacts at times $t = -\frac{\pi}{2\Omega} + \frac{mn\pi}{\Omega}$, $m \in \mathbf{Z}$. For even n, periodic orbits are neither of P nor T type but the simplest examples are of "peak-trough" (PT) type. For this case, the distance travelled between the walls does not depend on their amplitude, A.

A constant velocity motion ($\omega = 0$) case can be obtained by taking the limit $\omega \to 0$. The constant speed for the period-n periodic orbits becomes $y_0 = 2(1+A)\Omega/(n\pi)$ for T orbits and $y_0 = 2(1-A)\Omega/n\pi$, $A < 1$, for P orbits. For period-n PT orbits, $y_0 = 2\Omega/n\pi$.

3.2 Stability of period-n P- and T-orbits for $\omega = 0$

The trough-trough period-n motions with $t_0 = -\pi/(2\Omega)$ and $\hat{r} = 1$ for $\omega = 0$ give the following linearizations for each of the four dynamical equations which compose to give the linearised Poincaré map (cf. Appendix 1 and also Section 4.1, eqn. (26)):

$$\begin{aligned} \mathbf{J}^i(t_j) &= \begin{bmatrix} 1 & 0 \\ (1+r)A\Omega^2 & -1 \end{bmatrix}; & \mathbf{J}^f(t_j) &= \begin{bmatrix} 1 & -\frac{n\pi}{y_0} \\ 0 & 1 \end{bmatrix}; \\ \mathbf{J}^i(t_{j+1}) &= \begin{bmatrix} 1 & 0 \\ -(1+r)A\Omega^2 & -1 \end{bmatrix}; & \mathbf{J}^f(t_{j+1}) &= \begin{bmatrix} 1 & \frac{n\pi}{y_0} \\ 0 & 1 \end{bmatrix}. \end{aligned} \tag{10}$$

at consecutive impact times $t = t_j$ (lower) $t = t_{j+1}$ (upper).

The composition of the four matrices in (10) give the linearised Poincaré map

$$D\mathcal{P}(t_j, y_j^-) = \mathbf{F} = \mathbf{J}^f(t_{j+1})\mathbf{J}^i(t_{j+1})\mathbf{J}^f(t_j)\mathbf{J}^i(t_j). \tag{11}$$

We immediately observe that the matrix $\mathbf{F}$ obtained by composing the four '$\mathbf{J}$' matrices has determinant 1 and so eigenvalues of $\mathbf{F}$ are either hyperbolic or elliptic depending on whether or not $|\mathrm{Trace}(\mathbf{F})| \leq 2$. The trace of $\mathbf{F}$ has the following form in the period-n case:

$$\mathrm{Trace}(\mathbf{F}) = 2 - 16R + 16R^2 \tag{12}$$

where

$$R = \frac{n^2\pi^2 A}{4(1+A)} \tag{13}$$

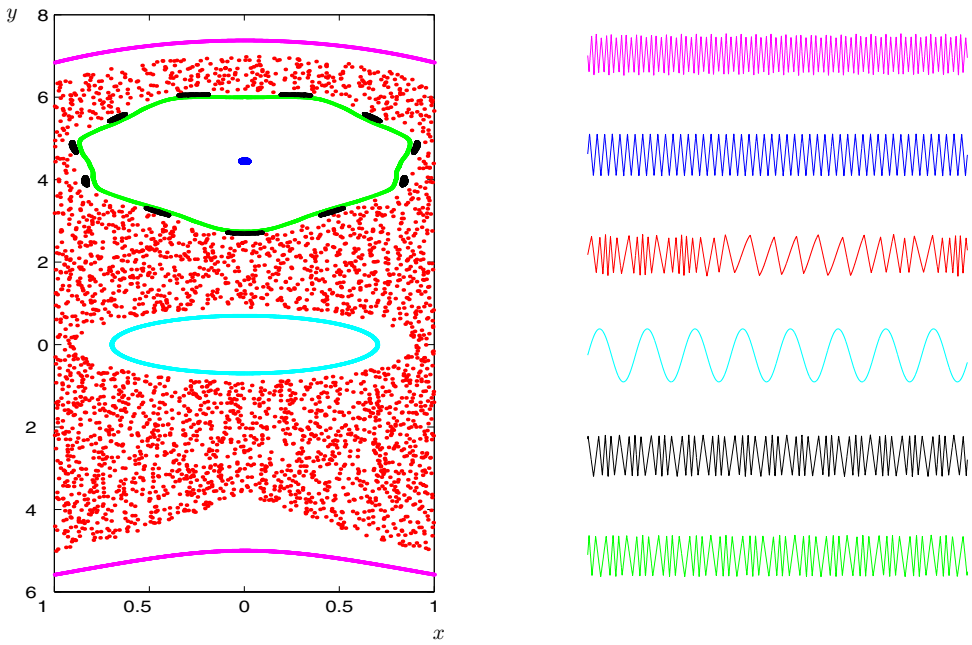

Figure 2: Various orbits from stroboscopic sampling at times $t = t_0 + 2\pi n/\Omega$ for $n \in \mathbb{Z}$ - (a) the motion in the Poincaré section xy-space; (b) the particle motion in xt-space with the wall motion omitted. The orbits of the same colour in (a) and (b) represent the same motion.

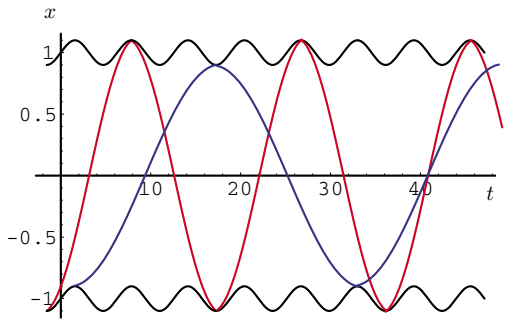

Figure 3: Examples of a period-3 T-orbit ($\omega/\Omega = 0.3$), and a period-5 P-orbit ($\omega/\Omega = 0.19$)

by using $n\pi/y_0 = n^2\pi^2/(2\Omega(1+A))$. The condition $|\text{Trace}(\mathbf{F})| < 2$ is satisfied if and only if $0 < R < 1$. Thus the upper limits of the stability regions for T-orbits in the ω, A-plane are given by the curve

$$A = \left(\frac{n^2\pi^2}{4} - 1\right)^{-1}. \tag{14}$$

when A is positive. Elliptical stability can be ensured by increasingly limiting the amplitude A as n is increased.

3.3 Stability of period-n P- and T- orbits for $\omega \neq 0$.

The symmetry conditions on the periodic orbits are the same as for the case $\omega = 0$ and defined by $\dot{W}_j = 0$, $\ddot{W}_{j+1} = (-1)^n \ddot{W}_j$ at subsequent impacts and the times of impact are $t_{j+1} = t_j + n\pi/(2\Omega)$. As noted in section 2, this scenario also requires $r = 1$ if $\beta = 0$, otherwise $r = \frac{(1+\beta)}{(1-\beta)}$ (with $\beta < 0$) to ensure $\hat{r} = 1$ in all cases. For period-n, we have the following Jacobians:

$$\begin{aligned}
J^i(t_j) &= \begin{bmatrix} 1 & 0 \\ -(1+r)\Omega^2 \sin\Omega t_j & -1 \end{bmatrix}, \\
J^f(t_j, t_{j+1}) &= \begin{bmatrix} 1 & -\frac{\sin(\omega\tau_j)}{\omega y_0} \\ 0 & 1 \end{bmatrix}, \\
J^i(t_{j+1}) &= \begin{bmatrix} 1 & 0 \\ -(1+r)\Omega^2 \sin\Omega t_{j+1} & -1 \end{bmatrix}, \\
J^f(t_{j+1}, t_{j+2}) &= \begin{bmatrix} 1 & \frac{\sin(\omega\tau_{j+1})}{\omega y_0} \\ 0 & 1 \end{bmatrix},
\end{aligned} \tag{15}$$

where the speed is $y_0 = \omega \cot(n\omega\pi/(2\Omega))$, and $\tau_j = t_{j+1} - t_j = n\pi/\Omega$.

Before considering controlling the system to either restore or abandon low-order periodicity, we consider the extent of uncontrolled stability in the parameter space for these resonant orbits. As for the case $\omega = 0$, we observe that the matrix $\mathbf{F}$ obtained by composing all four matrices has determinant 1 and so its eigenvalues are either hyperbolic or elliptic according as $|\text{Trace}(\mathbf{F})|$ is either greater or less than 2.

The trace of $\mathbf{F}$ has the form (12), where now

$$R = \frac{A\sin^2(\frac{n\pi\omega}{2})}{(1+A)\omega^2}. \tag{16}$$

Again, the condition $|\text{Trace}(\mathbf{F})| < 2$ is satisfied if and only if $0 < R < 1$. Thus the upper limit of the stability region in the ω, A-plane is given by the curve

$$A = \frac{1}{\frac{1}{\omega^2}\sin^2(\frac{n\pi\omega}{2}) - 1} \tag{17}$$

when A is positive. For the case $\omega \to 0$, we have $\sin^2(\frac{n\pi\omega}{2})/\omega^2 \to n^2\pi^2/4$ and eqn. (14) when $\omega = 0$ is recovered. The regions for elliptic behaviour as n-varies are shown in Fig. 4.

The trace and determinant constraints mean that we have stable but not asymptotically stable behaviour in these regions. This will result in an oscillatory (elliptic) behaviour around the trough-trough equilibrium, see Fig. 4. Note from Fig. 4 that for intervals of ω, we have that the stability boundary exists for sufficiently large amplitudes A. Above these boundaries the fixed points become saddle points. Thus for small A, we should be able to implement an arbitrarily small control with $\Delta\beta$ for which we can either asymptotically stabilize or destabilize the elliptic fixed point, by changing $\hat{r}$, the effective coefficient of restitution.

3.4 Grazing orbits

The above analysis is based on the assumption that successive impacts take place on alternate walls, i.e. that we have no multiple impacts on one wall. This assumption will not hold if an orbit of the particle is not physically possible; i.e. that the wall encroaches on the particle's path. The physical limit for these cases occurs when the particle undergoes a *grazing* impact with a wall as parameters are changed. That is the particle and the wall touch, but the particle does not suffer an impulse.

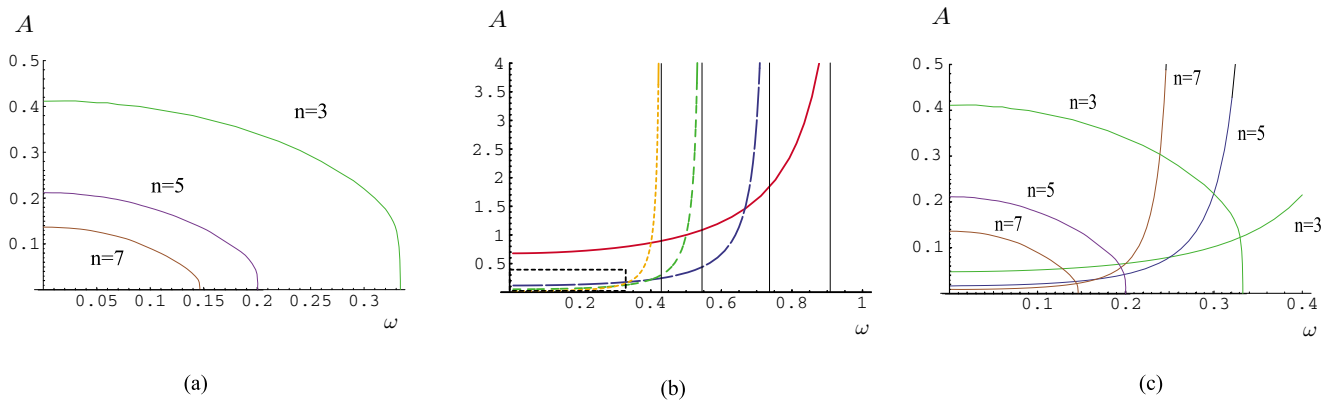

Figure 4: (a) The grazing bifurcation curves of period-n periodic orbits in the $\omega - A$ plane, with $\omega/\Omega = 0.33$, get closer to the origin with increasing $n = 3, 5, 7$. Grazing is the predominant feature for the break-up of resonant curves as the period n increases. (b) The stable(elliptic) regions for T orbits in the ω, A-plane (cf. equation (17)) with $n = 1, 2, 3, 4$ as dash size decreases. (c) The box in diagram (b) is enlarged to show the competing limits for stability and grazing.

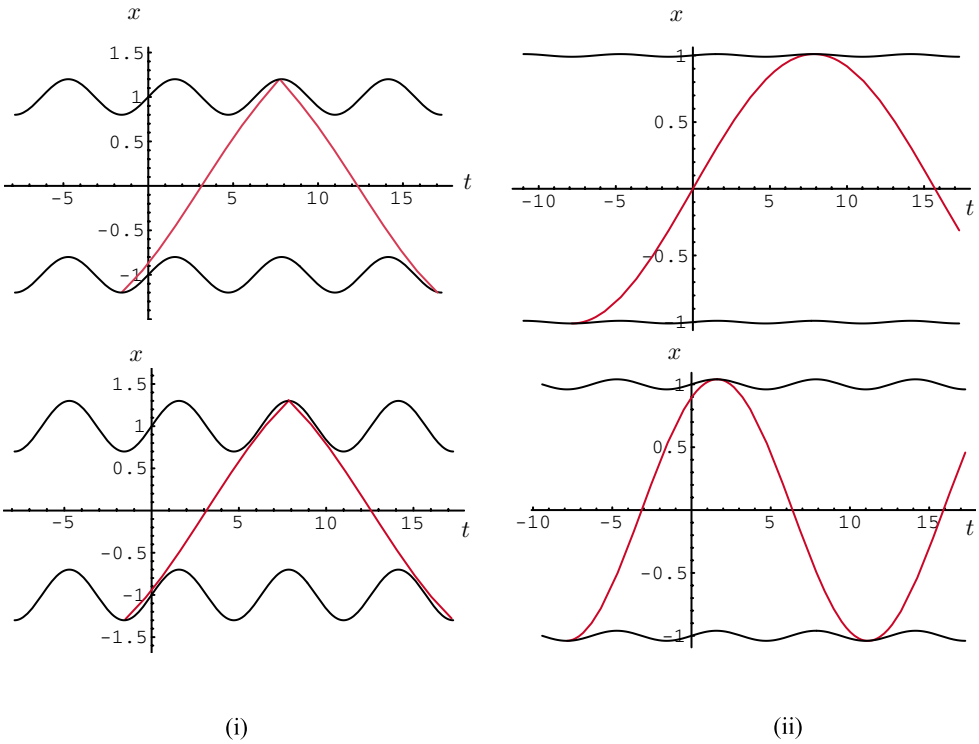

Figure 5: Examples of the grazing impacts periodic trough-trough orbits as the wall amplitude is increased for: (i) $n = 1$, and (ii) $n = 3$. The amplitudes in (i) are $A = 0.2, 0.3$ and in (ii) $A = 0.01, 0.04$. We observe that the grazing for $n = 1$ T-orbits occurs at much higher values of the wall amplitude A than for the $n = 3$ T- orbits.

3.4.1 The consequences of increasing wall amplitudes

Avoidance of grazing imposes further *severe* constraints on the admissible parameter points (ω, A) (see Figs 4 and 5). Typically the symmetric orbits described above only exist for wall amplitudes (A) sufficiently small to allow no grazing impacts other than those described above to take place. A simple observation is that alternate wall impacting scenarios can be realised when the walls do not oscillate, i.e. when the amplitude $A = 0$ and then no grazing can take place. As the amplitude of the wall oscillation increases, the likelihood of unhindered alternate wall bouncing decreases. In Fig. 5, it is seen that grazing terminates the periodic motion for $n = 3$ when A is increased, whereas in Fig. 4, the existence of symmetric orbits is shown to be less likely for a given fixed amplitude A as the period n of the orbit increases. The grazing limits on amplitude for trough-trough symmetric orbits when the periodicities $n = 1, 3, 5, 7$ are given in Fig. 4. For comparison, the boundaries of the regions for which the orbits are elliptic are also shown.

The behaviour of symmetric trough-trough period-1 periodic orbits as $\frac{\omega}{\Omega} \to 1$ allows for arbitarily large amplitudes without grazing. The reason is simply that the wall and particle motions increasingly synchronize their shapes. In this sense, the low-order resonance of a period-1 orbit is very persistent and not easily disturbed by grazing or *destabilization* of the equilibrium.

4 Control equations for resonant periodic orbits: $\omega = 0$

4.1 Time-symmetric periodic orbits

We now relax the space-symmetry and consider time-symmetric orbits in some detail. Time-symmetry alone requires that for period-n periodic orbits, impacts take place on alternate walls at the equally spaced times $t_j = t_0 + nj\pi/\Omega$, $i \in \mathbf{Z}$. First of all, we restrict to the simplest case of $\omega = 0$ in free flight. Time symmetry demands that the (constant) speed between walls remains constant after impacts. Thus, for periodic orbits to occur, the velocity needs to be maintained constant in amplitude at each impact, i.e, in equation (3) , the condition $y_0^+ = -y_0^- = y_0$ is required. We get

$$y_0 = \frac{(1+r)}{(1-\hat{r})}\dot{W}_r(t_0) = \frac{(1+r)}{(1-\hat{r})}A\Omega\cos\Omega t_0. \tag{18}$$

It follows from this equation that non-trivial periodic orbits can be maintained when $\dot{W}(t_0) = 0$ (that is $\cos\Omega t_0 = 0$) at impact only if $\hat{r} = 1$. This is the case of the T and P orbits referred to above and the wall impact offers no impulse and the velocity will decay by the factor $\hat{r} < 1$.

For $\dot{W}(t_0) \neq 0$, time-symmetric orbits exist provided equation (18) is satisfied.

For displacement feedback $\beta_0 \neq 0$, the requirement that a fundamental period-one orbit has constant speed y_0 over the freeflight time π/Ω implies that

$$y_0 = \{\, 2\Omega(1 - A\sin\Omega t_0)/(\pi(1-\beta)) \,. \tag{19}$$

For the n-th subharmonic, we have a slower speed of

$$y_0 = \begin{cases} 2\Omega(1 - A\sin\Omega t_0)/(n\pi(1-\beta)), & \text{for } n \text{ odd}, \\ 2\Omega/(n\pi(1-\beta)), & \text{for } n \text{ even}, \end{cases} \tag{20}$$

when $n > 1$. Thus the constraints for admissible initial conditions are given by equating the two values of the speed y_0 in (18) and (20).

Remark Another important aspect of the effective coefficient of restitution $\hat{r}$ is that its value can exceed unity for certain admissible choices of β_0. Thus displacement feedback and impact dissipation may be combined in an equivalent restitution parameter $\hat{r}$ which enables movement away from unwanted periodic orbits. In particular, the double impact system, with a fixed coefficient of restitution $r \leq 1$ and a negative feedback β_0, can undergo a Hopf bifurcation at a fixed point and this scenario will be considered elsewhere.

4.2 Linear control equations for displacement feedback

First of all, we consider perturbations of the period-one equilibrium point. The state of the system is given by the vector (t, y, β) at each given impact. The variable β drives the system and can be chosen arbitrarily at each

impact, although its choice determines the dynamical state. Let Δt, Δy^-, $\Delta\beta$ be the perturbations of the equilibrium time(t), the pre-impact velocity(y) and the displacement feedback(β) for each of the impact times $t = t_0, t_1$ and t_2 respectively. We take Δy_j^- and Δy_j^+ to denote velocities before and after an impact at $t = t_j$ and take $(\Delta y^-, \Delta t, \Delta\beta)$ at each impact to be the *state* of the system. The control mechanism is a perturbation $\Delta\beta_j$ from the equilibrium β_0 which is applied at time $t = t_j$.

The equilibrium conditions satisfy the constraints imposed by eqns (18) and (20) and the dynamical behaviour is derived from (i), the free-flight equation (2), and (ii), the impact equation (3). The variational free-flight equations are (i) for the interval $[t_0, t_1]$ (in general, $[t_j, t_{j+1}]$)) :

$$\begin{aligned} y_0(\Delta t_1 - \Delta t_0) + \frac{\pi}{\Omega}\Delta y_0^+ &= \frac{(1 + A\sin\Omega t_1)}{(1-\beta_0)^2}\Delta\beta_1 + \frac{A\Omega\cos\Omega t_1}{(1-\beta_0)}\Delta t_1 \\ &\quad - \frac{(-1 + A\sin\Omega t_0)}{(1-\beta_0)^2}\Delta\beta_0 - \frac{A\Omega\cos\Omega t_0}{(1-\beta_0)}\Delta t_0, \end{aligned} \tag{21}$$

and (ii) for the interval $[t_1, t_2]$ (in general, $[t_{j+1}, t_{j+2}]$) :

$$\begin{aligned} -y_0(\Delta t_2 - \Delta t_1) + \frac{\pi}{\Omega}\Delta y_1^+ &= \frac{(-1 + A\sin\Omega t_2)}{(1-\beta_0)^2}\Delta\beta_2 + \frac{A\Omega\cos\Omega t_2}{(1-\beta_0)}\Delta t_2 \\ &\quad - \frac{(1 + A\sin\Omega t_1)}{(1-\beta_0)^2}\Delta\beta_1 - \frac{A\Omega\cos\Omega t_1}{(1-\beta_0)}\Delta t_1. \end{aligned} \tag{22}$$

The variational impact equations are (a) $t = t_0$:

$$\Delta y_0^+ = -y_0(1+r)\Delta\beta_0 - \hat{r}\Delta y_0^- - (1+r)A\Omega^2\sin\Omega t_0\Delta t_0 \tag{23}$$

and (b) $t = t_1$:

$$\Delta y_1^+ = y_0(1+r)\Delta\beta_1 - \hat{r}\Delta y_1^- - (1+r)A\Omega^2\sin\Omega t_1\Delta t_1. \tag{24}$$

Given the sequence of feedback values $\{\beta_i\}$, then the wall position is determined exactly at impact by the time t_i. So we can interpret (t_j, y_j^-) as the state variables and the value $\beta_j = \beta_0 + \Delta\beta_j$ as the control variable. Thus the four equations enable a Poincaré map to be defined

$$(t_{j+2}, y_{j+2}^-, \beta_{j+2}) = \mathcal{P}_{\Delta\beta}(t_j, y_j^-, \beta_j) \tag{25}$$

where $\Delta\beta = (\Delta\beta_{j+1}, \Delta\beta_{j+2})$ for the return coordinates (t, y) at the subsequent impacts on the lower (or the upper) wall.

We will be considering control feedback of the form $\Delta\beta_i = \Delta\beta_i(\Delta t_{i-1}, \Delta y_{i-1}^-)$, for $i = j, j+1, \ldots$.

Using $\Delta t^+ = \Delta t^-$ at each impact $t = t_j$, we obtain, when $\omega = 0$, that the four linearised control equations for the various stages of motion are given by:

$$\mathbf{J}^i(t_j) = \begin{bmatrix} 1 & 0 \\ -(1+r)A\Omega^2\sin\Omega t_j & -\hat{r} \end{bmatrix}; \tag{26}$$

$$\mathbf{J}^f(t_j, t_{j+1}) = \begin{bmatrix} \frac{y_0(1-\beta_0) - A\Omega\cos\Omega t_j}{y_0(1-\beta_0) + A\Omega\cos\Omega t_j} & -\frac{\pi(1-\beta_0)}{(y_0(1-\beta_0) + A\Omega\cos\Omega t_j)} \\ 0 & 1 \end{bmatrix}; \tag{27}$$

$$\mathbf{J}^i(t_{j+1}) = \begin{bmatrix} 1 & 0 \\ -(1+r)A\Omega^2\sin\Omega t_{j+1} & -\hat{r} \end{bmatrix}; \tag{28}$$

$$\mathbf{J}^f(t_{j+1}, t_{j+2}) = \begin{bmatrix} \frac{y_0(1-\beta_0) + A\Omega\cos\Omega t_{j+1}}{y_0(1-\beta_0) - A\Omega\cos\Omega t_{j+1}} & \frac{\pi(1-\beta_0)}{(y_0(1-\beta_0) - A\Omega\cos\Omega t_{j+1})} \\ 0 & 1 \end{bmatrix}; \tag{29}$$

$$\mathbf{K}^i(t_j) = -\kappa_1 \begin{bmatrix} 0 & 0 & 0 \\ 1 & 0 & 0 \end{bmatrix};$$

$$\mathbf{K}^f(t_j, t_{j+1}) = \kappa_2 \begin{bmatrix} 1 & 1 & 0 \\ 0 & 0 & 0 \end{bmatrix};$$

$$\begin{aligned}\mathbf{K}^i(t_{j+1} &= \kappa_1 \begin{bmatrix} 0 & 0 & 0 \\ 0 & 1 & 0 \end{bmatrix}; \\ \mathbf{K}^f(t_{j+1}, t_{j+2}) &= \kappa_2 \begin{bmatrix} 0 & 1 & 1 \\ 0 & 0 & 0 \end{bmatrix};\end{aligned} \tag{30}$$

where $\kappa_1 = y_0(1+r)$. For the time-symmetric case we consider here with $t_{j+2} - t_{j+1} = t_{j+1} - t_j = \pi/\Omega$ the various partial derivatives of free flight times with respect to the controls β_i for $i = j, j+1, j+2$ are the same and given by

$$\kappa_2 = \frac{1 - A\sin\Omega t_j}{(1-\beta_0)(y_0(1-\beta_0) + A\Omega\cos\Omega t_j)}.$$

Remark It can be seen that in various stages of the motion, some of the controls have no effect. For example, in the impact at $t = t_j$, the controls β_{j+1}, β_{j+2} have no effect. All controls are included for ease of description so that *formally* each component of the dynamics has input from $\beta_0, \beta_1, \beta_2$. However, to obtain a consistent Poincaré map we assume the state $\mathbf{s_j} = (t_j, y_j, \beta_j)$ with feedback controls $\Delta\beta_{j+1}(\mathbf{s}_j), \Delta\beta_{j+2}(\mathbf{s}_{j+1})$, which determines the new state $\mathbf{s}_{j+2}$, and so on.

Thus, the linearised control equation for each of the four cases above is of the form

$$\begin{bmatrix} \Delta t' \\ \Delta y' \end{bmatrix} = \mathbf{J} \begin{bmatrix} \Delta t \\ \Delta y \end{bmatrix} + \mathbf{K} \begin{bmatrix} \Delta\beta_0 \\ \Delta\beta_1 \\ \Delta\beta_2 \end{bmatrix}. \tag{31}$$

By definition we have $\Delta y_j^+ = \Delta y_{j+1}^-$ and $\Delta y_{j+1}^+ = \Delta y_{j+2}^-$ and so, as observed above, we can express the state $(\Delta t_{j+2}, \Delta y_{j+2}^-)$ at $t = t_{j+2}$ in terms of the state $(\Delta t_j, \Delta y_j^-)$ at time $t = t_j$ and the displacement feedback controls $\Delta\beta_j, \Delta\beta_{j+1}, \Delta\beta_{j+2}$ by composing the four *affine* maps in (31) to obtain

$$\begin{bmatrix} \Delta t_{j+2} \\ \Delta y_{j+2}^- \end{bmatrix} = \mathbf{F} \begin{bmatrix} \Delta t_j \\ \Delta y_j^- \end{bmatrix} + \mathbf{G} \begin{bmatrix} \Delta\beta_j \\ \Delta\beta_{j+1} \\ \Delta\beta_{j+2} \end{bmatrix}. \tag{32}$$

Note that the matrix pair $[\mathbf{F}, \mathbf{G}]$ is obtained by affine composition of the four matrix pairs

$$[\mathbf{J}^f(t_{j+1}, t_{j+2}), \mathbf{K}^f(t_{j+1}, t_{j+2})], \quad [\mathbf{J}^i(t_{j+1}), \mathbf{K}^i(t_{j+1})],$$

$$[\mathbf{J}^f(t_j, t_{j+1}), \mathbf{K}^f(t_j, t_{j+1})], \quad [\mathbf{J}^i(t_j), \mathbf{K}^i(t_j)],$$

from the various stages of the motion between successive lower wall impacts.

5 Control of trough-trough periodic orbits

5.1 Trough-trough control equations

The trough-trough motion requires $r = (1+\beta)/(1-\beta)$ to ensure $\hat{r} = 1$. This is necessary because the wall has zero velocity at impact for P and T orbits and offers no impulse. Thus a *negative* feedback β is needed for physical admissibility. The matrix $\mathbf{G}$ in the linear control system (32) is given by,

$$\mathbf{G} = \begin{bmatrix} \kappa_2 + \frac{\pi}{y_0\Omega}(2\kappa_1 - \gamma_1) & 2\kappa_2 + \frac{\pi}{y_0\Omega}(\kappa_1 - (1+r)A\Omega^2\kappa_2) \\ \kappa_1 - \gamma_1 & \kappa_1 - (1+r)A\Omega^2\kappa_2 \end{bmatrix}, \tag{33}$$

where $\gamma_1 = (1+r)A\Omega^2(\kappa_2 + \kappa_1\frac{\pi}{y_0\Omega})$. The matrix $\mathbf{G}$ is generically of rank 2 (i.e. $\mathbf{G}^{-1}$ will exist) within the set of admissible choices of κ_1 and κ_2. If we consider the problem of choosing $\Delta\beta_0$ and $\Delta\beta_1$ such that

$$|(\Delta t_2, \Delta y_2^-)| < |(\Delta t_0, \Delta y_0^-)|, \tag{34}$$

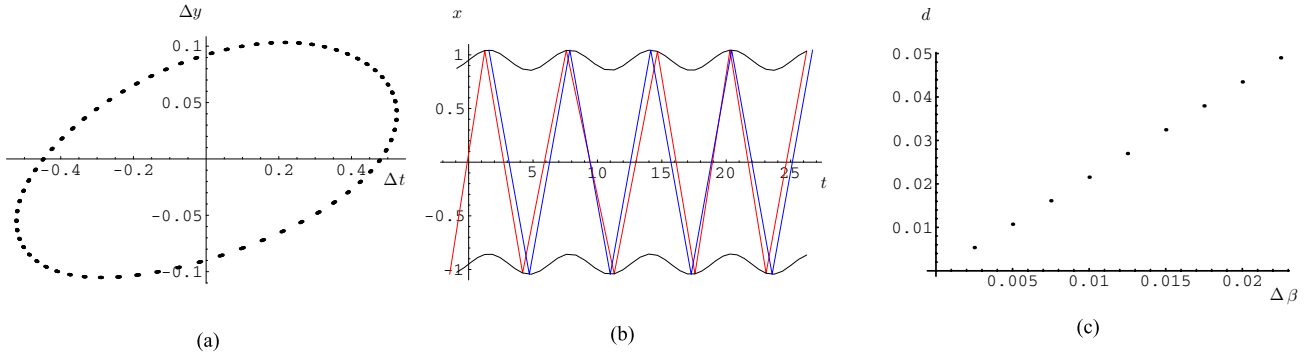

(a) (b) (c)

Figure 6: (a) The elliptic nature of the period-1 double impact orbit $(\Delta t, \Delta y) = (0.1, 0.1)$ for a T-orbit in the Poincaré (t, y) plane with $t_0 = -\pi/2$, $y_0^- = -0.700282$, $\Omega = 1$, $r_0 = 0.9$, $\hat{r} = 1$, $A = 0.1$; (b) the same orbit(red) is shown impacting the walls and oscillating around the fixed period-1 orbit (blue). (c) The numerical dependence of the displacement $d = |\xi|$, the perturbation of a period-1 T-orbit on $\Delta\beta \in [0, 0.025]$ when $(A, \Omega, r, \beta_0) = (0.5, 1.0, 1.0, 0)$. A least squares fit of the graph is $d = 2.17816\Delta\beta - 0.00014$ (within 2% error of the true value obtained from eqn (40)).

then

$$\begin{bmatrix} \overline{\Delta\beta_0} \\ \overline{\Delta\beta_1} \end{bmatrix} = -\mathbf{G}^{-1}\mathbf{F} \begin{bmatrix} \Delta t_0 \\ \Delta y_0^- \end{bmatrix} \tag{35}$$

restores the equilibrium of $(\Delta t_0, \Delta y_0^-) = \underline{0}$, at the linear level, in a single iteration.

Control using displacement feedback perturbations at just one wall can also be implemented. If we consider the case of a Poincaré map obtained from bottom wall impacts, then the control using $\Delta\beta_1$ at the impact with the upper wall impact with no action at the lower wall (i.e. setting $\Delta\beta_0 = \Delta\beta_2$=0) gives

$$\mathbf{G}_u = \begin{bmatrix} 2\kappa_2 + \frac{\pi}{y_0\Omega}(\kappa_1 - (1+r)A\Omega^2\kappa_2) \\ \kappa_1 - (1+r)A\Omega^2\kappa_2 \end{bmatrix}. \tag{36}$$

Note that $\mathbf{G}(\neq \mathbf{0})$ is not an eigenvalue of $\mathbf{F}$ thus making the controllability matrix $[\mathbf{G}, \mathbf{FG}]$ have full rank. Then the system is completely controllable using upper wall controls alone, i.e $\Delta\beta_i \equiv 0$ for i even. By contrast, if the control mechanism is not sufficiently responsive to be changed for alternating walls at high frequencies we can consider a *constant* control with $\Delta\beta_i = \Delta\beta$, say, for all integers i and we obtain

$$\mathbf{G}_a = \begin{bmatrix} 4\kappa_2 + \frac{\pi}{y_0\Omega}(3\kappa_1 - (1+r)A\Omega^2(2\kappa_2 + \kappa_1\frac{\pi}{y_0\Omega})) \\ 2\kappa_1 - (1+r)A\Omega^2(2\kappa_2 + \kappa_1\frac{\pi}{y_0\Omega}) \end{bmatrix}. \tag{37}$$

5.2 Numerical validation of the matrices F and G

We consider the case of T-orbits and obtain the dependence of the size of the perturbed fixed point of the *constant* double impacting control $\Delta\beta$ at each impact by using the linearised equation (26). Sufficiently small *fixed* perturbations of the displacement feedback β from its equilibrium value results in a perturbed periodic orbit which will, if sufficiently small, remain stable (see Fig. 2). Assume that the fixed point $s_0 = (t_0, y_0)$ for $\beta = \beta_0$ of the Poincaré return map, P, to the lower wall map is perturbed to $s = s_0 + \xi$ by the perturbation of displacement feedback $\beta = \beta_0 + \Delta\beta$ at every impact, then on linearizing the map $\mathcal{P}$ we have

$$\xi = F(s_0, b_0)\xi + G_c(s_0, b_0) \begin{bmatrix} 1 \\ 1 \end{bmatrix} \Delta\beta \tag{38}$$

which implies

$$\xi = [I - F(s_0, b_0)]^{-1} G_c(s_0, b_0) \begin{bmatrix} 1 \\ 1 \end{bmatrix} \Delta\beta. \tag{39}$$

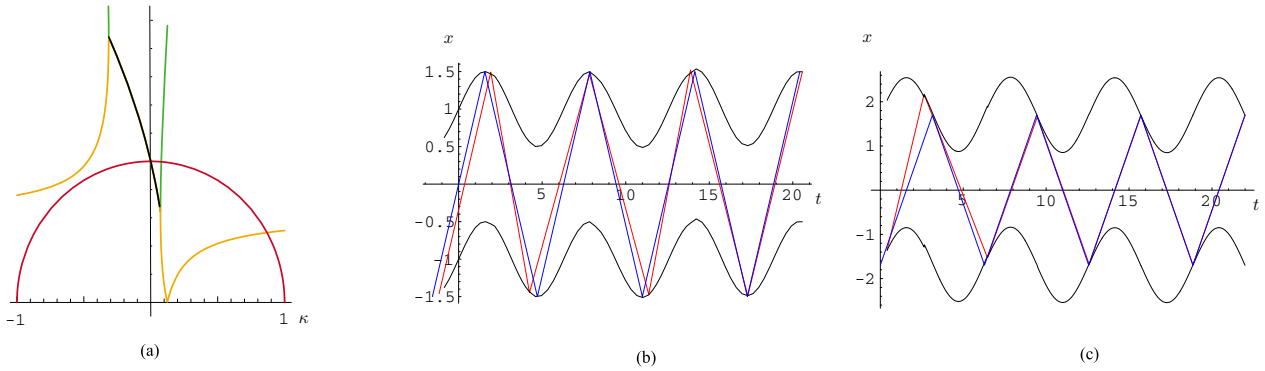

Figure 7: (a) The eigenvalue behaviour as a function of κ. The two moduli have common values on the black segment where the eigenvalues are complex conjugate. For small positive κ we have stability. (b) Control to the desired period-1 T-orbit using $\Delta\beta = \kappa(\Delta y + \Delta t)$ with $\kappa = 0.03$. (c) Similar controls are successful for **non** T-orbits, e.g. $(A, r, \beta) = (0.5, 0.9, 0.41)$ and a target fixed point $(t_0, y_0^-) = (0, -1.07979)$. The initial perturbation was $(\Delta t_0, \Delta\beta) = (0.4, 0.5)$.

Assuming the fixed perturbation, consider the case of a constant velocity T-orbit with $(A, r, \beta, \Omega) = (0.5, 1.0, 0.0, 1.0)$ the linearised control equations are

$$\mathbf{F} = \begin{bmatrix} 1.95362 & -4.24349 \\ 1.28987 & -2.28987 \end{bmatrix}; \qquad \mathbf{G} = \begin{bmatrix} -5.87352 \\ -5.60506 \end{bmatrix}.$$

The resulting fixed point perturbation matrix in equation (39) for the constant $\Delta\beta = \Delta\beta_i$ is given by

$$\xi = \begin{bmatrix} 1.90986 \\ -0.95493 \end{bmatrix} \Delta\beta, \tag{40}$$

and so $|\xi| = 2.13529|\Delta\beta|$, (cf. Fig. 6).

5.3 Linear control of period-1 periodic orbit

Numerical experiments are based on the actual equations of motion and not the linearised control equations. Nevertheless, the linearised control solution for the numerical stabilization of a period-1 orbit for the numerical case described in subsection 5.2 can be successfully applied. We restrict to the simplest control law for the case in eqn (37) which is $\Delta\beta = \kappa(\Delta y + \Delta t)$, (cf. Fig. 6).

The moduli of the two eigenvalues of $\mathbf{F} + \mathbf{GK}$ where $\mathbf{K} = \kappa\,[1 \quad 1]^T$ for κ in a neighbourhood of 0 are given in Fig. 7(a). For $\kappa \in (0, 0.075)$ the feedback will stabilize the orbit. The behaviour and control illustrated here for $A = 0.5$ can be repeated for the amplitude range $A \in (0, 0.681)$. An equal weight, κ has been applied to each of the variables $\Delta t, \Delta y$ of the linear feedback control. This balance can be refined according to the relative costs of errors Δy and Δt.

In Fig. 8, the orbits are plotted in *time-velocity* coordinates and we have a sample of the elliptic (stable) behaviour for low-amplitude wall oscillations around the fixed point corresponding to the fundamental period-1 periodic orbit.

5.4 Control of period-n periodic orbit

The linear controls described for period-1 orbits can be simply adapted for all periods n. The displacement feedback equation (39) can be exploited to provide a state-feedback which stabilises the equilibrium (t_0, y_0^-) for appropriate κ.

We show here that a nonlinear feedback control

$$\Delta\beta_{i+1} = -\kappa\sqrt{(\Delta t_i^2 + \Delta y_i^2)} \tag{41}$$

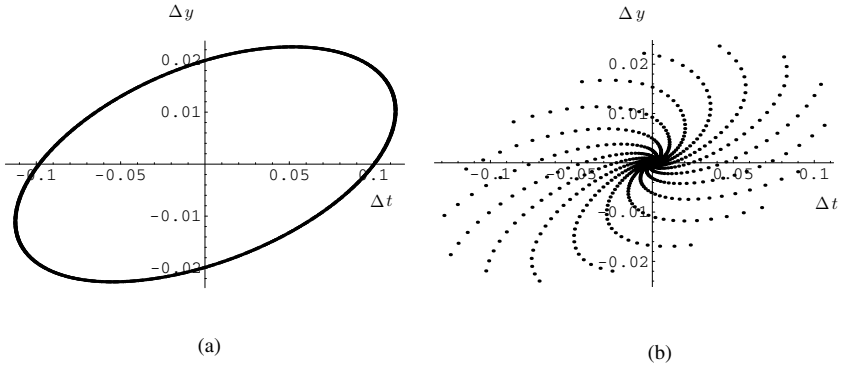

(a) (b)

Figure 8: (a) The uncontrolled behaviour around the fixed point $(t_0, y_0^-) = (-\pi/2, -0.95493)$ showing its elliptic nature with $r = \hat{r} = 1$, and (b), the effect of a fixed perturbation $\Delta\beta_0 > 0$ which also asymptotically stabilizes the system by forcing $\hat{r} < 1$. The change in β_0 by $\Delta\beta_0 = 0.1$ has the effect of perturbing to a nearby fixed point $(t_0, y_0^-) = (-1.62775, -0.996679)$.

can serve as an effective feedback for stabilizing periodic orbits. The displacement feedback equation (39) can be exploited to provide a state-feedback which stabilises the system at an equilibrium close to the target period-3 point (t_0, y_0^-). Specifically, we can employ the control in eqn. (41) for appropriate κ, (see Fig. 9) which provides an asymptotically exponential decay to the equilibrium. Consider the case $(\Omega, A, r, \beta) = (1.0, 0.5, 1.0, 0.0)$ which has a stable period-1 orbit at $(t_0, y_0^-) = (-\pi/2, -0.95493)$ which provides an asymptotically exponential decay to the equilibrium. The equilibrium wall-wall oscillation is denoted by the blue line in Fig. 9 onwards and the red line is the actual dynamical oscillation to be controlled.

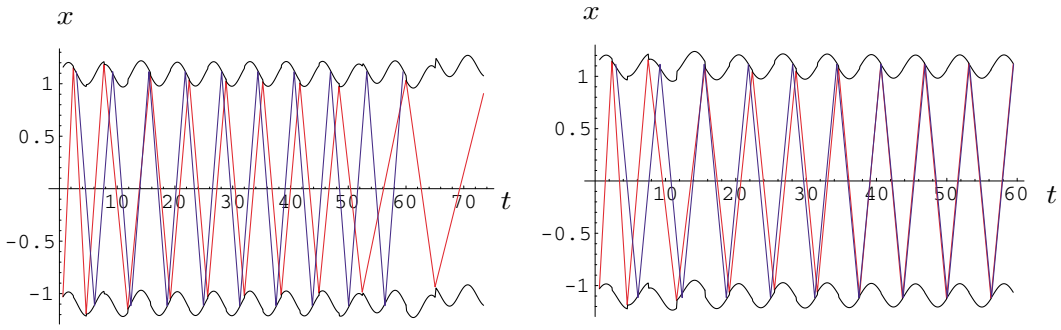

(a) (b)

Figure 9: Feedback control of a period-1 orbit for $(A, r, \beta_0) = (0.1, 0.9, 0.08542)$, $(\hat{r} = 1)$ using (41) with (a) $\kappa = 0.0$, (b) $\kappa = 0.01$, (c) $\kappa = 0.02$. The large initial perturbation from the equilibrium $(t_0, y_0^-) = (0.2, -0.70991)$ is $(\Delta t_0, \Delta y_0^-) = (0.8, 0.5)$ from the equilibrium. The uncontrolled instability (a) is transiently marginalised (b) permanently controlled.

It should be noted that the above choice of a sufficiently small constant control $\Delta\beta_0 > 0$ will always change an elliptic fixed point (with $r = \hat{r} = 1$) into a nearby asymptotically fixed point when $\hat{r} < 1$.

The same behaviour occurs for a period-n fundamental orbit for trough-trough oscillations, the equilibrium condition is obtained from the case $n = 1$ by *reducing* the velocity by a factor n while the time is *increased* by the same factor n. Elliptic behaviour of orbits around the fixed point and controllability by using displacement feedback is shown in Fig. 8. It should be noted that this behaviour is restricted to smaller regions of the ω, A plane than for the case $n = 1$ (cf. Fig. 4 and 5).

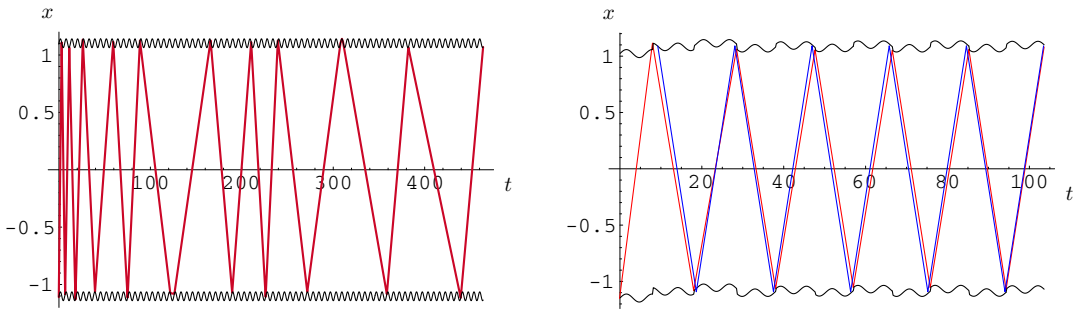

(a) (b)

Figure 10: Stability and control near a period-3 periodic orbit for $(A, r, \beta) = (0.031, 0.9, -0.052)$ and : (a) the unstable nature of the period-3 T-orbit at $(\Delta t, \Delta y) = (0, 0)$ with initial perturbation $(0.1, 0.05)$ and $\Delta\beta = 0.05$; (b) the unstable behaviour with no control $\kappa = 0$ is asymptotically stabilised for $\kappa = 0.2$ in eqn(41).

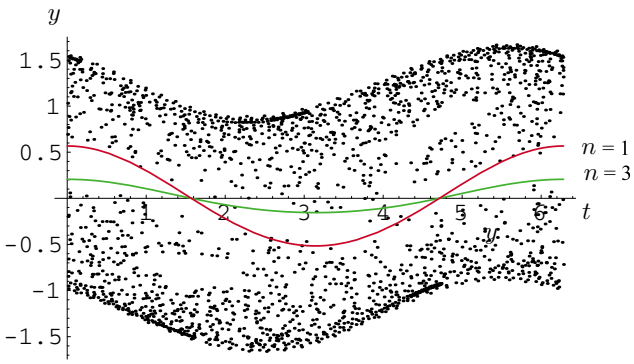

Figure 11: A chaotic orbit in ty-space can be controlled to a low-velocity orbit by applying local feedback control as described in subsection 5.4. The chaotic orbit is sufficiently close to a constant velocity orbit for periods n=1,3, etc. The lines labelled by n are the sets of initial conditions for the impact coordinates (t, y) that give rise to constant speed period-n motion.

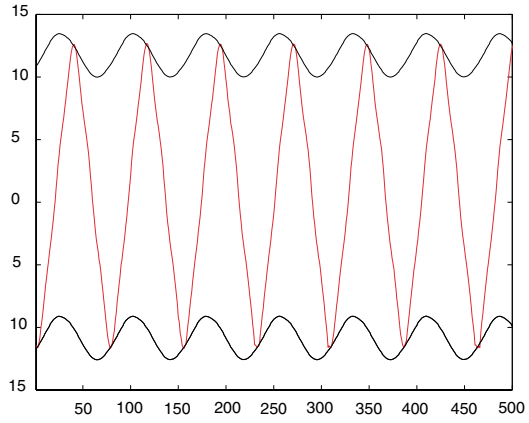

Figure 12: A stable period-1 resonant impact orbit

5.5 Resonance avoidance and anti-chaos control

The previous sections have dwelt on the low order resonant behaviour, [6]. The bench apparatus that is being modelled here has desirable behaviour away from resonance orbits cf. [26].

We have seen in section 3.4 that periodic orbits, period-n, for $n \geq 3$, are highly sensitive to grazing bifurcations as the wall amplitude is increased. Thus it is usually possible to change from a stable resonant orbit by a transient increase in wall motion amplitude which can be implemented by adjusting the displacement feedback β. This has already been discussed in section 3.4 and can be seen as anti-control whereby a sufficient change in β changes the wall position for multiple impact on one wall. Repeated application of this procedure is likely to give rise to an orbit in the chaotic regime of Fig. 2. Here we see that the likelihood of chaotic motion in the stroboscopic phase plane appears to be substantial.

Conversely, it is possible within chaotic regions to move close to regular orbits, as we demonstrate in Fig. 11 . In this situation, the chaotic regime orbits can be brought to low-velocity resonance using the OGY two-step method of (i) allowing the chaotic orbit to get near to a chosen resonant orbit, and then, (ii) apply the local controls used above to obtain periodic behaviour, see [19, 25]. Note that the higher the resonance period, the lower the particle velocity between impacts and therefore the less energy is expended in impacting. This makes the higher order resonances less problematical although they can be addressed in the same way as for period 1 periodic orbits in Fig. 11 . Techniques for extracting the local linear control equations from orbital measurements also exist [19, 25] and would be equally appropriate in this problem to obtain numerical control equations.

5.6 Engineering applications of anti-chaos control: examples from the laboratory

We now return to the original motivation for this study after providing a dynamical systems approach to the stability and control of impact vibrations associated with doubly constrained discontinuous mechanical systems. In practical engineering terms non-linear resonances are no different from linear ones: they either serve a purpose or must be eliminated. Impact resonances cause unnecessary wear or, in the case of servo-hydraulic machinery, imprecise positioning or undesirable impulsive loading. In particular, periodic orbits with n round trips per single oscillation of the wall for large n are most serious as they are associated with high impact velocities. Moreover, such orbits can have large basins of attraction and are stable for extensive subsets of the parameter space. Thus, whereas for most dynamical theoreticians, chaotic regimes are often of great interest, statistically over a time series, they are associated with lower impact speeds and hence, are more benign than low order impact resonances. However, it is often the case that non-linear resonances in mechanical equipment are not well-diagnosed and hence are their effects are mitigated by heuristic, 'black-box', approaches.

We now provide some examples of low order resonances obtained from measurements of laboratory experiments on a spring-mass impact oscillator, see Fig. 1(b), and discuss how they may be eliminated using a dynamical systems approach with similarities to the approach developed for the numerical model discussed in the preceding sections.

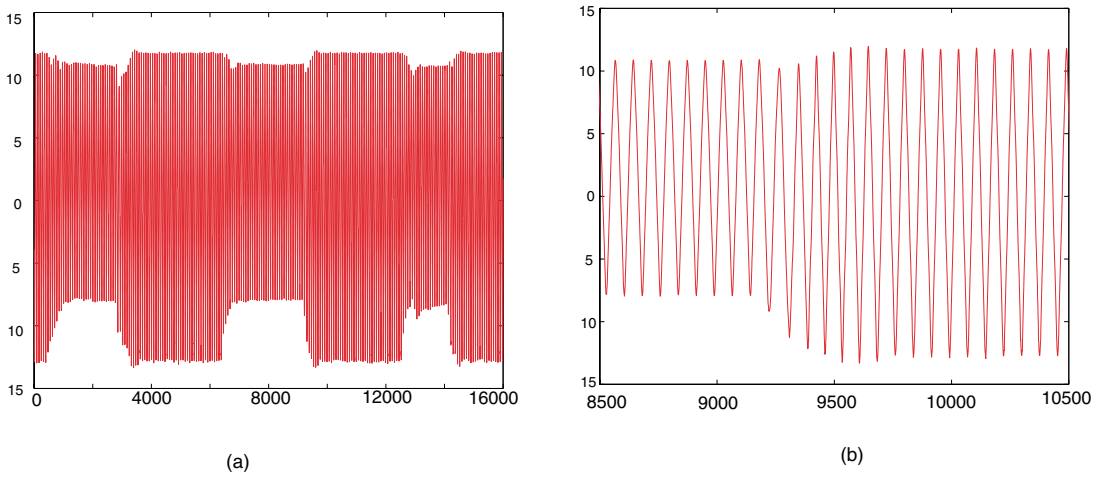

Figure 13: (a) Perturbations of a period 1 orbit impact orbit; (b) detail of a perturbation of a period 1 orbit.

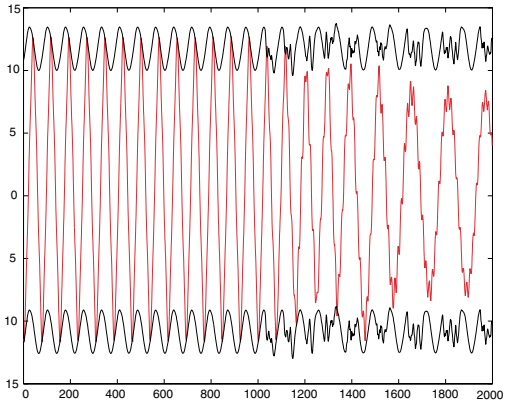

Figure 14: Anti-control of a period-1 periodic impact orbit onto an impact-less orbit.

A laboratory bench model Fig 1(a) of a doubly constrained impact oscillator, kinematically equivalent to that described in Fig. 1(b), was designed and tested with a view to reproducing the analytical behaviour described above. It is important to note the main differences between the experimental and the analytical models and consider how these may affect our interpretation of the results. The bench model experiment has many degrees of freedom –these will be observed in the experimental times series as high order mechanical vibrations superimposed on the main time series of the particle motion. Moreover, control commands are not executed instantly because the control system has inherent action delay time as it, too, is a mechanical system. In addition to these problems, the differential quantities used in control, for example velocity, are measured from noisy mechanical signals, for this reason the control is preformed in delay coordinates of the stroboscopic Poincaré section rather than in the time,velocity t, y-space for the sequential impacts used for the analytical and numerical investigations in this paper. We leave for a forthcoming paper [9] discussions of the implications that these aspects may have within the context of non-linear control theory. For the present, the following examples are meant to motivate further research whilst at the same time giving an indication of how a dynamical systems methodology, even if imperfectly applied, is consistent with observed behaviour up to experimental error.

An example of an experimental period-1 orbit is shown Fig. 12. The walls are moving at a frequency of 13 Hz whereas the natural frequency of the oscillator is 6.3 Hz, hence $\frac{\omega}{\Omega} \simeq= 0.485$. The figure reproduces the ensemble of wall and particle motions, however, each electronic signal is measured independently, thus the signal is reconstructed

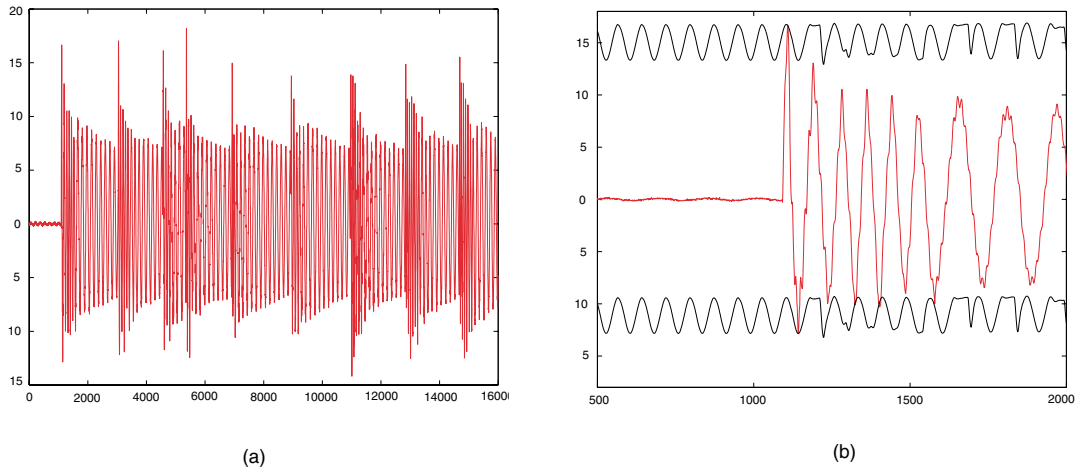

Figure 15: (a) Inhibition of (1,1) orbits by continuous anti-control; (b) detail of inhibition of anti-control

by matching the displacements (here the physical units are in mm) of the top and bottom walls and the particle signal at the time of a given impact (a point in the time series coinciding with a peak of displacement of the particle signal). Of course matching times and displacements of one specific impact in the time series does not ensure that impact reconstructions will match exactly for all the prior and subsequent impacts of the time series, for as in any real system, drift in the signals will shift the location of the impact position and consequently, in Fig. 12 some of the particle impacts appear to pierce the wall when clearly this did not happen in the bench experiment.

Prior to the application of the control algorithm the perturbations of the periodic orbit were measured in order to quantify the spectral quantities. The period-1 periodic orbits shown in Fig. 13(a) and Fig. 13(b) are perturbed by reducing the gap size with an obstacle: the orbit returns quickly to the original fixed point consistent with a heavily damped 2D system. The continuation of the $(1,1)$ resonance is shown in Fig. 14, where at approximately time point 1000 the control is switched on. The feedback was performed by varying the frequency of motion of the walls coinciding with the fixed point of the stable periodic orbit measured in delay coordinates xi, x_{i-1} taken from a stroboscopic Poincaré map. The initial control schemes were not effective. It was subsequently realised that the delay of the piston controller in executing the desired command effectively resulted in the generation of the command signal far away from the desired fixed point in state space. Based on the measured actuation delay times of the servo-hydraulic system, the delay co-ordinates were re-set to account for the piston delay time. The result of applying the anti-control algorithm eliminates the impact orbit and generates an impact-less oscillation that decays in time – the non-impact decay rate being dependent on the viscous internal hysteretic damping capacity of the spring mass system which is not considered in the numerical model considered above. The application of anti-control may be extended in a pre-trigger mode: i.e. the control is always active and monitors state space for incipient resonances, in this case for a period one resonance, this is shown in the particle time series of Fig. 15(a). The data shows how at certain points a large impulse is applied to the particle which, under normal circumstances would usually set off a period 1 resonance (these points are marked by the intermittent sharp spikes at the start of the oscillation segments). It can be seen that the system is inhibited from resonance by the intervention of the controller. A detail of the particle and wall motion is shown in Fig. 15(b) (note that the time series of walls and particle shown are matched only for one specific point in the time series). The figure is only meant to indicate the general behaviour of the effect the control algorithm has on the walls: as explained earlier perfect graphical matching of the representation of the kinematics of the walls and particle at impact is not possible. As a reference we show the acceleration signal of the particle which was measured from an accelerometer mounted on the oscillator mass, Fig. 16(a).

The accelerometer reading highlights the impacts more clearly whereas the impact-less oscillations are of smaller magnitude. In a close up (see Fig. 16(b)) the impact set starts with the kick-start impacts and continues with a series of impact spikes which progressively reduce in magnitude. The last impact spike, with negative acceleration, is associated with a low velocity -quasi-grazing- impact. The impact-less motion before and after the impact set is characterised by the natural vibrations of the mechanical system, the signal shows clearly the superposition of the two main modes: in general the impacts excite the higher modes. Nevertheless, in spite of this behaviour the

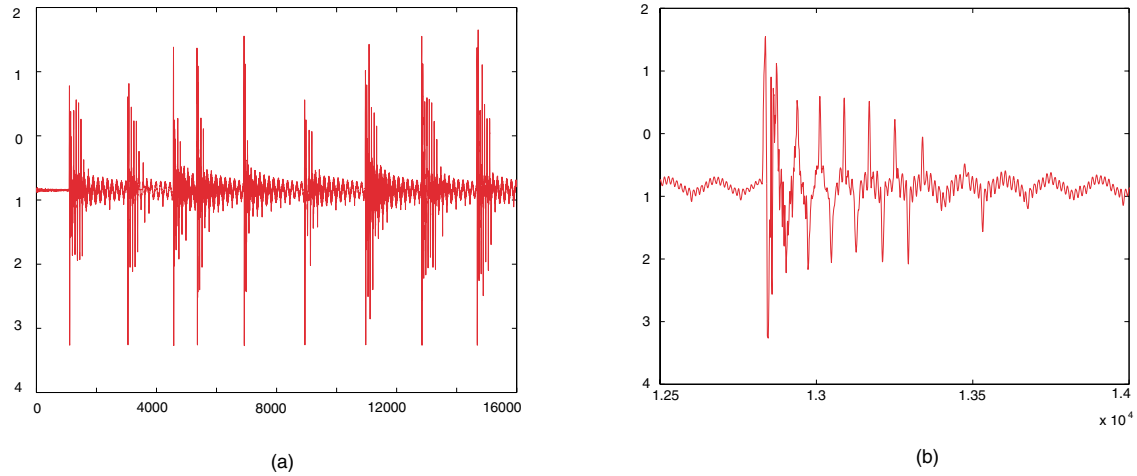

Figure 16: (a) Inhibition of (1,1) orbit seen by accelerometer signal; (b) detail of (1,1) inhibition by the accelerometer.

predominant behaviour of the oscillator is condensed as a single-degree-of-freedom. This observation is important when considering future investigations and highlights the remarks made by some authors [3] as to the importance of appropriately considering such aspects as the extraction of data using time series analysis techniques and the influence of condensation of system dimensionality in the case of dissipative impact systems.

6 Conclusions

A dynamical systems approach has been applied to investigate the nature of some non-linear resonances in complex, multi-actuated, servo-hydraulic structural engineering applications. In order to study such systems it was first necessary to condense the system dimensionality by realizing simple –single-degree-of-freedom– numerical and experimental models. The stability of low order impact resonances has been studied on such models in the context of the application of control techniques using displacement feedback. The resonant orbits of dissipative numerical oscillators that are deemed to be of interest in engineering applications of non-linear control theory have been reproduced in the experimental bench model. Control schemes based on the OGY [19] scheme have been applied to both numerical and experimental models. It was noted that whereas the numerical model is defined as having one degree-of-freedom and that of the experimental system was shown to contain multiple oscillation modes, the dissipative nature of impact resonances reduces the essential dynamics in both cases making it possible to apply a low dimensional analysis. Based on these observations, we propose for further study that the resonances in multiply-actuated systems may essentially be dominated by low order non-linear modes as is the case in the experiments shown here.

Acknowledgements. E. Gutierrez would like to thank the Exploratory Research Programme of the IPSC at the European Commission Joint Research Centre (Ispra) for the original funding of part of this study.

References

[1] B. Blazejczyk-Okolowska, F. Peterka, An investigation of the dynamic system with impacts, *Chaos, Solitons & Fractals* **Vol 9**, No 8, 1998 1321–1338.

[2] A. Brahic, Numerical Study of a simple dynamical system. *Astron. Astrophys* **12**, 1971, 98-110.

[3] C. Budd, F. Dux and A. Cliffe, The effect of frequency and clearance variations on single-degree-of-freedom impact oscillators, *J. Sound and Vibration.* **184**(3), 1995,475-502.

[4] C. Budd, F. Dux, Intermittency in impact oscillators close to resonance. *Nonlinearity* **7** 1994, 1191–1224.

[5] J.A. Chen, K. Suykens, T. Yang, J. Vandewalle and L.O. Chua, Impulsive Control and Synchronization of Chaos. *Controlling Chaos and Bifurcations in Engineering Systems, ed. G. Chen, CRC Press*, 275–292.

[6] W. L. Ditto, S. N. Rauseo and M. L. Spano, Experimental Control of Chaos, *Phys. Rev. Lett.* **65**,(1990), 3211 .

[7] J. Guckenheimer and P.J. Holmes, *Nonlinear Oscillations, Dynamical Systems and Bifurcations of Vector Fields.* Springer Verlag, New York, 1983, 102–116.

[8] E. Gutiérrez, G. Magonette, J. Molina, D. Tirelli, G. Verzeletti, Methodology for the vibration-isolation testing of full-scale structures fitted with rate dependent rubber bearings Proc. 1st European Conf. On Struc. Control, 306-313, 1996, World Sci. Press.

[9] E. Gutierrez and D.K. Arrowsmith, Scaling phenomena of chaotic attractors in experimental and numerical impact oscillators. (*in preparation*).

[10] H. Hu, Controlling chaos of a dynamical system with discontinuous vector field, **Physica D 106**, 1997, 1-8

[11] A.P. Ivanov, Bifurcations in impact systems, *Chaos, Solitons & Fractals* **Vol 7**, No 8, 1998 No 10, 1615–1634.

[12] G.X. Li, R.H. Rand, F.C. Moon, Bifurcations and Chaos in a Forced Zero-Stiffness Impact Oscillator. *Int. J. Non-Linear Mechanics*, **25** No. 4, pp. 417 - 432, 1990.

[13] A.C.J. Luo and R.P.S. Han, The dynamics of a Bouncing Ball with a Sinusoidally Vibrating Table. *Nonlinear Dynamics* **10** 1996, 1–18.

[14] G. Luo and J. Xie, Bifurcations and chaos in a system with impacts, *Physica D*, **148** (2001) 183-200.

[15] G. Magonette, Development and application of large-scale continuous pseudo-dynamic testing techniques, *Phil. Trans R. Soc. London. A* **359**, 2001, 1771-1799.

[16] S.A. Mahin and P.B Shing, Pseudodynamic method of seismic testing, *J. Struct. Engrg. ASCE,* **111***(7)* 1987, 1482-1503.

[17] A. Nordmark, Non-periodic motion caused by grazing incidence in an impact oscillator, *J. Sound and Vibration* **145**, 1991, 279-297.

[18] H.E. Nusse and J.A.Yorke, Border-collision bifurcations including period 2 to period 3 for piecewise smooth systems *Physica D* **57**, 1992, 39-57.

[19] E. Ott, C. Grebogi and J.A. Yorke, Controlling Chaos, *Phys. Rev. Letts.* **64 11** 1990 1196-1199.

[20] M. Paskota, On the modelling and the control of vibroformers in aluminium production *Chaos, Solitons & Fractals* **Vol 9**, No 1/2, 1998, 323–335.

[21] S.W.Shaw, The Dynamics of a harmonically excited system having rigid amplitude constraints:Part 1 Chaotic motions and global bifurcations, *J. of Applied Mechanics, Transactions of ASME*,**Vol. 52**, 1985, 453-458.

[22] S.W.Shaw, The Dynamics of a harmonically excited system having rigid amplitude constraints:Part 2 Subharmonic motions and local bifurcations, *J. of Applied Mechanics, Transactions of ASME*, **Vol. 52**, 1985, 459-464.

[23] S.W. Shaw, R. H. Rand, The transition to chaos in a simple mechanical system, *Int. J. Non-linear Mechanics*, **Vol. 24, No 1**, 1989, 41–56.

[24] S.W. Shaw and P.J. Holmes, A Periodically Forced Piecewise Linear Oscillator, *Jnl. Sound and Vibration.* **90**(1), 1983,129-155.

[25] T.L. Vincent & A.I. Mees, Controlling a bouncing ball. *Int Jnl of Bifurcation and Chaos.*, **10** No. 3 (2000), 579–592. 579-592.

[26] V. Visarath, S.E. Mahan, W.L. Ditto, M.L. Spano, Experimental maintenance of chaos, *Phys Rev. Lett.***74** (1995) pp. 4420-4423.

APPENDICES

Appendix 1: Linearised control equations for general system

The coordinates for describing the dynamical behaviour can be taken as the time of impact(t), and velocity of impact(y^-). The impact equation (3) gives a jacobian

$$J^i(t_0) = \frac{\partial(t_0, y_0^+)}{\partial(t_0, y_0^-)} = \begin{bmatrix} 1 & 0 \\ -(1+r)\ddot{W}(t_0) & -\hat{r} \end{bmatrix}. \tag{42}$$

The equations for the corresponding free-flight Jacobian are much more complex. They are obtained implicitly from equations (2) and (5). The Jacobian matrix

$$J^f(t_0, t_1) = \frac{\partial(t_1, y_1^-)}{\partial(t_0, y_0^+)} \tag{43}$$

has coefficients

$$\frac{\partial t_1}{\partial t_0} = \frac{A\Omega\cos\Omega t_0\cos(\omega\tau_0) + \omega(-1 + A\sin\Omega t_0)\sin(\omega\tau_0) - y_0^+(1-\beta_0)\cos(\omega\tau_0)}{A\Omega\cos\Omega t_1 - y_0^+(1-\beta_0)\cos(\omega\tau_0) + \omega(-1 + A\sin\Omega t_0)\sin(\omega\tau_0)} \tag{44}$$

$$\frac{\partial t_1}{\partial y_0^+} = \frac{(1-\beta_0)\sin(\omega\tau_0)}{\omega(A\Omega\cos\Omega t_1 - y_0^+(1-\beta_0)\cos(\omega\tau_0) + \omega(-1 + A\sin\Omega t_0)\sin(\omega\tau_0))} \tag{45}$$

$$\frac{\partial y_1^-}{\partial t_0} = -\omega\left(\frac{A\Omega\cos\Omega t_0\sin(\omega\tau_0)}{(1-\beta_0)} - (\frac{\partial t_1}{\partial t_0} - 1)\left(\frac{\omega\cos(\omega\tau_0)(-1 + A\sin\Omega t_0)}{(1-\beta_0)} + y_0^+\sin(\omega\tau_0)\right)\right) \tag{46}$$

$$\frac{\partial y_1^-}{\partial y_0^+} = \cos(\omega\tau_0) - \frac{\partial t_1}{\partial t_0}\omega\left(\frac{\omega\cos(\omega\tau_0)(-1 + A\sin\Omega t_0)}{(1-\beta_0)} + y_0^+\sin(\omega\tau_0)\right), \tag{47}$$

where $\sin(\omega\tau_0) = \sin(\omega\tau_0)$ and $\cos(\omega\tau_0) = \cos(\omega\tau_0)$ with $\tau_0 = t_1 - t_0$.

The "overall" jacobian for a fundamental periodic orbit is given by the product

$$J^f(t_1, t_2)\cdot J^i(t_1)\cdot J^f(t_0, t_1)\cdot J^i(t_0) \tag{48}$$

where $t_2 = t_0 + 2\pi/\Omega$.

Appendix 2: Piecewise-constant speed periodic behaviour

We relax the time symmetry and allow the components of the periodic orbit to be the constant speed y_0^+ from the bottom to top wall and y_0^- in the reverse direction. These speeds are not necessarily equal.

The linearised $\mathbf{J}$ matrices of the Poincaré map $\mathcal{P}$ given in (26) for the time-symmetric (constant speed) case take the more general form:

$$\begin{aligned}
\mathbf{J}^i(t_0) &= \begin{bmatrix} 1 & 0 \\ -(1+r)A\Omega^2\sin\Omega t_0 & -\hat{r} \end{bmatrix}; \\
\mathbf{J}^f(t_0, t_1) &= \begin{bmatrix} \frac{y_0^+ - \mu_0}{y_0^+ - \mu_1} & -\frac{\tau_i}{y_0^+ - \mu_1} \\ 0 & 1 \end{bmatrix}; \\
\mathbf{J}^{i+1}(t_1) &= \begin{bmatrix} 1 & 0 \\ -(1+r)A\Omega^2\sin\Omega t_1 & -\hat{r} \end{bmatrix}; \\
\mathbf{J}^f(t_1, t_2) &= \begin{bmatrix} \frac{y_0^- - \mu_1}{y_0^- - \mu_0} & -\frac{\tau_{i+1}}{y_0^- - \mu_0} \\ 0 & 1 \end{bmatrix};
\end{aligned}$$

where

$$\mu_0 = \frac{A\Omega\cos\Omega t_0}{(1-\beta_0)}, \qquad \mu_1 = \frac{A\Omega\cos\Omega t_1}{(1-\beta_0)},$$

Note that we have substituted $y_1^- = y_0^+$ and $y_1^+ = y_0^-$ for the free flight during $[t_1, t_2]$. The two impact equations are

$$y_0^+ = -\hat{r}y_0^+ + (1+r)A\Omega\cos(\Omega t_0)$$

at time $t = t_0$ on the lower wall, and

$$y_0^- = -\hat{r}y_0^+ + (1+r)A\Omega\cos(\Omega t_1)$$

at time $t = t_1$ on the upper wall. We obtain

$$y_0^- = \frac{(1+r)A\Omega(\cos\Omega t_1 - \hat{r}\cos\Omega t_0)}{1-\hat{r}^2}$$

and

$$y_0^+ = \frac{(1+r)A\Omega(\cos\Omega t_0 - \hat{r}\cos\Omega t_1)}{1-\hat{r}^2}.$$

and it can be deduced that

$$\frac{(y_0^+ - \mu_0)}{(y_0^+ - \mu_1)} = \frac{(y_0^- - \mu_1)}{(y_0^- - \mu_0)} = \hat{r};$$

It follows that the composite Jacobian

$$\mathbf{F} = \mathbf{J}^f(t_1, t_2)\mathbf{J}^{i+1}(t_1)\mathbf{J}^f(t_0, t_1)\mathbf{J}^i(t_0)$$

gives

$$\mathrm{Det}(\mathbf{F}) = \hat{r}^4. \tag{49}$$

The special time-symmetric case where $t_1 = t_0 + \pi$ reduces to

$$y_0 = y_0^- = -y_0^+ = \left(\frac{1+r}{1-\hat{r}}\right)\dot{W}_r(t_0) = \left(\frac{1+r}{1-\hat{r}}\right)A\Omega\cos\Omega t_0. \tag{50}$$

This speed is also constrained by the time of flight and the distance between the walls. For a period-n piecewise-constant periodic orbit, we require

$$y_0^+(t_1 - t_0) = \frac{2 + A\sin\Omega t_1 - A\sin\Omega t_0}{1-\beta_0} = -y_0^-(2n\pi/\Omega - (t_1 - t_0)). \tag{51}$$

The composite Jacobian

$$\mathbf{F} = \mathbf{J}^f(t_1, t_2)\mathbf{J}^{i+1}(t_1)\mathbf{J}^f(t_0, t_1)\mathbf{J}^i(t_0)$$

gives

$$\mathrm{Det}(\mathbf{F}) = \hat{r}^2\left(\frac{y_0 - \mu_0}{y_0 + \mu_0}\right)\left(\frac{y_1 - \mu_1}{y_1 + \mu_1}\right). \tag{52}$$

It is worth noting that for non T- and P- orbits with $\mu_0 \neq 0$ we obtain

$$y_0 + \mu_0 = \frac{2(1+r)A\Omega\cos\Omega t_0}{(1-\hat{r})(1-\beta)}; \qquad y_0 - \mu_0 = \frac{2\hat{r}(1+r)A\Omega\cos\Omega t_0}{(1-\hat{r})(1-\beta)}$$

and thus

$$\frac{y_0 - \mu_0}{y_0 + \mu_0} = \hat{r}.$$

It follows that the constant velocity Jacobian in eqn (52) satisfies $\mathrm{Det}(\mathbf{F}) = \hat{r}^4$, see also [4] for an analogous result.

The composite Jacobian

$$\mathbf{F} = \mathbf{J}^f(t_1, t_2)\mathbf{J}^{i+1}(t_1)\mathbf{J}^f(t_0, t_1)\mathbf{J}^i(t_0)$$

gives

$$\mathrm{Det}(\mathbf{F}) = \hat{r}^2 \left(\frac{y_0 - \mu_0}{y_0 + \mu_0} \right)^2. \tag{53}$$

The case of P- or T- orbits gives $\mu_0 = 0$ which gives $\mathrm{Det}(\mathbf{F}) = \hat{r}^2$ where, as was noted, $\hat{r} = 1$. This can be seen directly from eqns (10).

We now have the possibility of linear asymptotic stabilization by ensuring that $\hat{r} < 1$, i.e. by choosing β appropriately, in the stable eigenvalue case. The non-square part of the discriminant in the formulae for the eigenvalues of $\mathbf{F}$ is given by

$$D = \sin \Omega t_0 (8\hat{r} y_0 + A\Omega^2 \pi (1 + r)(1 + \hat{r}) \sin \Omega t_0). \tag{54}$$

If $\sin \Omega t_0 < 0$, then

$$8\hat{r} y_0 + A\Omega^2 \pi (1 + r)(1 + \hat{r}) \sin \Omega t_0 > 0$$

for sufficiently small A, and hence the motion is asymptotically stable if $\hat{r} < 1$ and elliptic if $\hat{r} = 1$. Thus we can ensure linear stabilization by taking $\hat{r} < 1$. By contrast, if $\sin \Omega t_0 > 0$, then

$$8\hat{r} y_0 + A\Omega^2 \pi (1 + r)(1 + \hat{r}) \sin \Omega t_0 > 0$$

is also positive for all amplitudes $A > 0$, and hence the motion is either asymptotically stable or saddle-like if $\hat{r} < 1$.